Int. J. Multiphase Flow Vol. 13, No. 2, pp. 173–198, 1987
Printed in Great Britain.

0301-9322/87 $3.00 + 0.00

DEVELOPMENTS IN THE MODELLING OF HORIZONTAL ANNULAR TWO-PHASE FLOW

P. W. JAMES,[1] N. S. WILKES,[2] W. CONKIE[3] and A. BURNS[4]

[1]Department of Mathematics and Statistics, Plymouth Polytechnic, Drake Circus, Plymouth, Devon, England

[2]Engineering Sciences Division, AERE Harwell, Didcot, Oxfordshire, England

[3]Department of Physics, Queens University, Kingston, Ontario, Canada

[4]Department of Computer Science, University of Bradford, Bradford, W. Yorks, England

(*Received* 3 *January* 1985; *in revised form* 19 *September* 1986)

Abstract—Several authors have considered the extension from vertically upward flow to horizontal flow of a model for annular two-phase flow which allows separate descriptions of liquid droplet deposition and entrainment. However, solutions to the equations which result have either not been obtained or have been found to be mathematically and physically unacceptable. In this paper it is shown how to obtain acceptable solutions. In addition, various physical mechanisms which could improve the model are assessed. Of these it is shown that a variable deposition flux could lead to significant improvement between theory and experiment. A model for the variable deposition flux is then developed and is shown to give results at least in qualitative agreement with known experimental results. The inclusion of the variable deposition rate in the governing equations leads to encouraging results for film thickness and film flowrate distributions.

1. INTRODUCTION

Whalley *et al.* (1974) presented a theoretical model of annular two-phase flow, in a vertical heated round tube, which predicted the onset of dryout of the liquid film, and hence the critical heat flux, with an accuracy comparable with that of existing correlations. An essential feature of the model is the inclusion of separate descriptions of the processes of liquid droplet deposition and entrainment. Since that time the model has been developed to the point where it can be applied to nuclear reactor rod-bundles and transient flows (Whalley *et al.* 1978).

The success of the model in vertical flow has led a number of authors to investigate its applicability to horizontal annular two-phase flow. This flow regime occurs in a range of industrial processes, for example in the steam generating plant of nuclear power stations, where the need to predict dry-spots is important for the prevention of corrosion. Butterworth (1972), Hutchinson *et al.* (1974) and Fisher & Pearce (1978) have looked at the problem of fully-developed, adiabatic horizontal annnular two-phase flow but only Fisher & Pearce (1978) obtained solutions to the model equations for liquid film thickness and liquid film flowrate. Although their solutions show reasonable agreement between theory and experiment for the liquid film thickness at the top and bottom of the tube, the agreement for the distributions of liquid film thickness and liquid film flowrate around the tube is less satisfactory. In addition, the above authors found it necessary to adopt an assumption about the nature of the flow near the bottom of the tube in order to avoid solutions for the liquid film thickness distribution in which "spikes" (i.e. discontinuities in the liquid film thickness or its gradient) occurred.

More recently, Laurinat *et al.* (1985) have developed a model for horizontal annular two-phase flow in which momentum transfer, in addition to mass transfer, is allowed for. These authors obtain solutions to the model equations which do not exhibit spikes at the tube bottom. They also conclude that the circumferential interfacial shear stress is primarily responsible for the distribution of film thickness over the upper part of the tube.

The purpose of this work is to re-examine the application of the mass-transfer model of vertical annular flow to horizontal annular flow. In particular, the nature of the "spikes" at the bottom of the tube is examined, by working with a simplified model, and various mechanisms which could improve the agreement between the predictions from the model and experiments are assessed. It is found that if a variable deposition rate is incorporated into the model then better agreement

between theory and experiment should result. A major part of the paper is, therefore, concerned with the development of a model for the droplet deposition flux which can exhibit the required variation around the tube circumference.

Finally, the influence of the model for variable deposition rate on the prediction of liquid film thickness and liquid film flowrate distributions is assessed by incorporating it into the simple model for the flow derived previously.

2. FORMULATION OF THE CIRCUMFERENTIAL FLOW PROBLEM

We consider the problem of steady, fully developed, adiabatic, incompressible annular two-phase flow through a horizontal tube of radius R, in which droplet deposition and entrainment take place (see figure 1). The assumption of steady flow is a gross over-simplification of the real flow in the liquid film, which is turbulent and on which a range of surface disturbances propagate. Any results obtained from the model equations can therefore only represent mean flow properties.

With reference to cylindrical polar coordinates (r, θ, z) in which $\theta = 0$ defines the upward vertical and in which all dependent variables, except pressure, are independent of z, the radial and circumferential momentum equations, and the continuity equation, for the liquid film may be written

$$\rho\left(V_r\frac{\partial V_r}{\partial r}+\frac{V_\theta}{r}\frac{\partial V_r}{\partial \theta}-\frac{V_\theta^2}{r}\right)=-\rho g\cos\theta-\frac{\partial p}{\partial r}-\frac{1}{r}\frac{\partial \tau}{\partial \theta}, \quad [1]$$

$$\rho\left(V_r\frac{\partial V_\theta}{\partial r}+\frac{V_\theta}{r}\frac{\partial V_\theta}{\partial \theta}+\frac{V_r V_\theta}{r}\right)=\rho g\sin\theta-\frac{1}{r}\frac{\partial p}{\partial \theta}-\frac{1}{r^2}\frac{\partial}{\partial r}(r^2\tau) \quad [2]$$

and

$$\frac{1}{r}\frac{\partial}{\partial r}(rV_r)+\frac{1}{r}\frac{\partial V_\theta}{\partial \theta}=0. \quad [3]$$

In the above equations V_r and V_θ are the radial and circumferential components of velocity, ρ is the liquid density, p is the pressure, g is the acceleration due to gravity and τ is the circumferential shear stress. Normal stresses and their derivatives have been neglected. For the thin films which occur in annular two-phase flow it is more convenient to work with the coordinates

$$x = R\theta, \quad y = R - r, \quad [4]$$

and with velocities

$$u = V_\theta, \quad v = -V_r. \quad [5]$$

The variables are now scaled by means of characteristic length scales L and δ, and velocity scales, U and V, in the x- and y-directions, respectively. We write

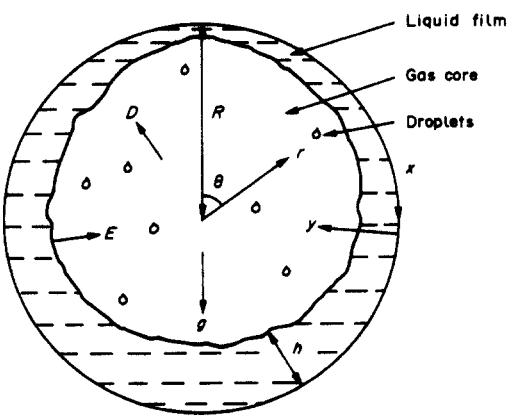

Figure 1. Sketch of horizontal annular flow.

$$x' = \frac{x}{L}, \quad y' = \frac{y}{\delta}, \quad u' = \frac{u}{U}, \quad v' = \frac{v}{V}, \quad p' = \frac{p}{\rho U^2} \quad \text{and} \quad \tau' = \frac{\delta\tau}{U\mu_T}, \tag{6}$$

μ_T being the effective turbulent viscosity for flow in the film. The continuity equation leads to the estimate

$$V = \frac{\delta U}{L}, \tag{7}$$

and if we neglect terms of order y/R and δ/R compared with unity then [1]–[3] may be written

$$\left(\frac{\delta}{L}\right)\left(u'\frac{\partial u'}{\partial x'} + v'\frac{\partial u'}{\partial y'}\right) = -\left(\frac{\delta}{L}\right)\frac{\partial p'}{\partial x'} + \frac{1}{\mathrm{Re}}\left(\frac{L}{\delta}\right)\frac{\partial \tau'}{\partial y'} - \frac{2\tau'}{\mathrm{Re}} + \left(\frac{g\delta}{U^2}\right)\sin\theta, \tag{8}$$

†

$$\left(\frac{\delta}{L}\right)^2\left(u'\frac{\partial v'}{\partial x'} + v'\frac{\partial v'}{\partial y'}\right) = -\frac{\partial p'}{\partial y'} - \frac{1}{\mathrm{Re}}\frac{\partial \tau'}{\partial x'} + \frac{g\delta}{U^2}\cos\theta \tag{9}$$

and

$$\frac{\partial u'}{\partial x'} + \frac{\partial v'}{\partial y'} = 0. \tag{10}$$

In [8] and [9] Re is a Reynolds number for circumferential flow in the film, defined by

$$\mathrm{Re} = \frac{LU}{(\mu_T/\rho)}. \tag{11}$$

The boundary conditions to be satisfied by [8]–[10] are

$$u' = v' = 0 \quad \text{at} \quad y' = 0, \tag{12}$$

$$v' + \frac{D - E}{\rho V} = u'\frac{\mathrm{d}h'}{\mathrm{d}x'} \quad \text{at} \quad y' = h' \tag{13}$$

and

$$p = p_s' \quad \text{at} \quad y' = h'. \tag{14}$$

Here D and E are the superficial deposition and entrainment mass fluxes, h' $(=h/\delta)$ is the non-dimensional local film thickness and p_s' $(=p_s/\rho U^2)$ is the non-dimensional local surface pressure. The inclusion of the deposition–entrainment term in [13] accounts correctly for mass transfer but not for momentum transfer.

The above equations are not, of course, sufficient to solve the circumferential flow problem; they must be coupled to the equations governing the axial flow. However, we postpone discussion of the axial flow until solutions for the various distributions are obtained. Instead, we examine the above set of equations in detail.

2.1. The Simplified Problem

If, in [8] and [9] we assume $L \sim R$, so that $\delta/L \ll 1$, then the inertia terms on the l.h.s. may be neglected together with the pressure gradient term in [8]. From [8] it is then seen that either $\mathrm{Re}^{-1} \sim g\delta/U^2$ or $\mathrm{Re}^{-1} \sim (g\delta/U^2)\,(\delta/L)$. The first possibility is rejected on the grounds that it leads to τ constant throughout the film and, since the boundary condition $\tau_s = 0$ will be imposed later, zero shear stress throughout the film would then result. The second estimate of Re^{-1} is therefore adopted and [9] then leads to $\mathrm{Re}^{-1} \sim \delta/L$, $g\delta/U^2 \sim 1$. In dimensional form the circumferential flow problem may now be written

$$0 = \frac{\partial \tau}{\partial y} + \rho g \sin\theta, \tag{15}$$

$$0 = -\frac{\partial p}{\partial y} + \rho g \cos\theta, \tag{16}$$

†Both x and θ are sometimes used in the same equation for ease of presentation.

$$\frac{\partial u}{\partial x}+\frac{\partial v}{\partial y}=0, \qquad [17]$$

$$u=v=0 \text{ at } y=0, \qquad [18]$$

$$v+\frac{D-E}{\rho}=u\frac{\mathrm{d}h}{\mathrm{d}x} \text{ at } y=h \qquad [19]$$

and

$$p=p_s \text{ at } y=h. \qquad [20]\dagger$$

If we assume that variations in gas pressure have negligible effect on the flow in the liquid film, because $\rho_G/\rho \ll 1$, where ρ_G is the gas density, then we may take p_s to be a constant. Equation [16] then gives

$$p=p_s-\rho g\,(h-y)\cos\theta. \qquad [21]$$

Integration of [17] from $y=0$ to $y=h$ gives, using [18] and [19],

$$\frac{\mathrm{d}}{\mathrm{d}\theta}(h\bar{u})=\frac{R[D-E(h)]}{\rho}, \qquad [22]$$

where

$$h\bar{u}=\int_0^h u\,\mathrm{d}y \qquad [23]$$

and we have taken the droplet deposition flux to be constant and assumed E to be dependent on h only. From [15] we have

$$\tau_s-\tau_w=-\rho g h\sin\theta, \qquad [24]$$

and if $\tau_s=0$, in other words secondary circumferential flows in the gas phase are ignored, then, by taking the local circumferential velocity distribution to be parabolic, we find

$$\bar{u}=\frac{\rho h^2 g\sin\theta}{3\mu_T}. \qquad [25]$$

Finally, combining [22] and [25] we obtain

$$\frac{\mathrm{d}}{\mathrm{d}\theta}(h^3\sin\theta)=\frac{3\mu_T R}{\rho^2 g}[D-E(h)]=F(h), \quad \text{say.} \qquad [26]$$

Equation [26] determines the circumferential film thickness distribution provided that a boundary condition for h can be found. The natural boundary conditions require $\bar{u}=0$ at $\theta=0$ and at $\theta=\pi$ but these are automatically satisfied by [25] provided that h remains finite. However, if we assume that $\mathrm{d}h/\mathrm{d}\theta\sin\theta\to 0$ as $\theta\to 0$ then [26] provides the boundary condition

$$h=h_0 \quad \text{at} \quad \theta=0, \qquad [27]$$

where

$$h_0^3=F(h_0). \qquad [28]$$

Equation [26] can now be solved numerically for $h(\theta)$ but it is found that $\mathrm{d}h/\mathrm{d}\theta$, and sometimes h, becomes very large as θ approaches π (see figure 2). This behaviour is also reported by Fisher & Pearce (1978) who refer to the growth in h as a cusp. The actual equation solved by Fisher & Pearce appears more complicated than [26] since they assume that the local circumferential velocity profile in the film is given by the universal profile. This complication has no relevance to the appearance of cusps, or spikes. Although Fisher & Pearce (1978) overcome this difficulty at the bottom of the tube by effectively stopping the integration well before the tube bottom is reached, it is felt essential to understand why spikes occur in the first place. There is nothing in the model

†Suffices s and w will be used to denote values at the surface of the film and at the tube wall, respectively.

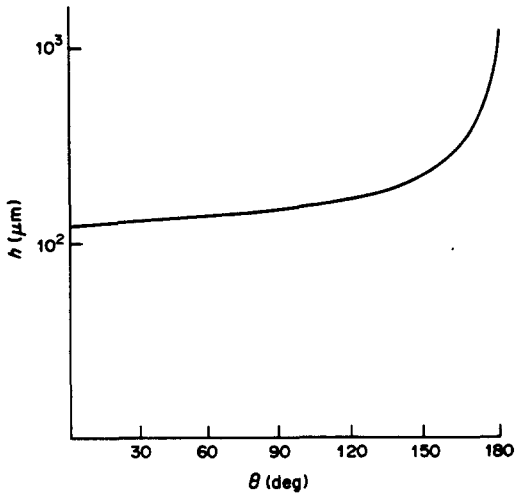

Figure 2. Typical solution of [26].

equations which makes them more applicable at $\theta = 0$ than at $\theta = \pi$, and in fact, by assuming that $dh/d\theta \sin\theta \to 0$ as $\theta \to \pi$, we could obtain a starting condition for the integration of [26] as

$$h = h_\pi \quad \text{at} \quad \theta = \pi, \tag{29}$$

where

$$h_\pi^3 = -F(h_\pi). \tag{30}$$

Thus the solution of [26] is not straightforward: it is investigated in more detail in section 2.2.

It is noted that the order of magnitude analysis leading to [15] and [16] relies on the assumption that h and $dh/d\theta$ scale as δ and that $\delta/L \ll 1$. If solutions to the simplified problem are obtained in which either h or $dh/d\theta$ is large at the bottom of the tube then this assumption is inconsistent and the solution of the simplified problem is meaningless physically. In section 2.5 we consider briefly different estimates for δ/L which result in a more complex set of model equations but in which it is still assumed that h or its gradient are not large at $\theta = \pi$. Here we consider a different question: can the addition of a term $\rho g\, dh/dx \cos\theta$ to the r.h.s. of [15] result in physically acceptable solutions (i.e. with $dh/d\theta = 0$ at $\theta = \pi$) which are not solutions of the simplified problem? There may of course be solutions which are not physically acceptable in which $dh/d\theta$ is finite at $\theta = \pi$. Laurinat *et al.* (1985) retain this term in their model but find from their numerical solutions that it has negligible importance. We show, in the following section, that it is possible to obtain physically acceptable solutions to the simplified problem, i.e. with the term $pg\, dh/d\theta \cos\theta$ omitted, and these solutions are similar, at least qualitatively, to those obtained by Laurinat *et al.* (1985). It is therefore not necessary to include this term to achieve physically acceptable solutions. For this reason, we have not investigated further the possibility that there are physically acceptable solutions to the unsimplified problem which are not solutions of the simplified problem.

2.2. The Nature of the Solutions of [26]

Since, at the moment, we have constant D for the circumferential flow problem, we may rewrite [26] as

$$\frac{d}{d\theta}(\eta \sin\theta) = 1 - f(\eta), \tag{31}$$

where

$$\eta(\theta) = h^3(\theta)/H^3, \tag{32}$$

$$H^3 = \frac{3\mu_T RD}{\rho^2 g} \tag{33}$$

and

$$f(\eta)=\frac{E(\eta)}{D}. \qquad [34]$$

We now assume that $E(\eta)/D$ can be written in the simple form $\lambda\eta$. At this stage, all that can be said in defence of this representation is that enables progress to be made in the examination of the solutions of [31]. But, it is stressed that this simple form can be given some justification from a physical viewpoint (see section 4) and will be retained for future calculations. With this simplification [31] can be solved exactly to give

$$\eta(\theta)=\frac{1}{\sin\theta\,\tan^{\lambda}\left(\frac{\theta}{2}\right)}\int_0^{\theta}\tan^{\lambda}\left(\frac{t}{2}\right)\mathrm{d}t. \qquad [35]$$

Writing

$$T=\tan\frac{\theta}{2}, \qquad [36]$$

we have

$$\eta(T)=\frac{1+T^2}{T^{\lambda+1}}\int_0^{T}\frac{t^{\lambda}}{1+t^2}\mathrm{d}t, \qquad [37]$$

which is a more appropriate form in which to examine the behaviour of η as $\theta\to 0$ and $\theta\to\pi$. For small values of θ, i.e. as $T\to 0$, [37] gives

$$\eta(T)\sim\frac{1}{\lambda+1},\quad \lambda\neq -1 \qquad [38]$$

and so η and all its derivatives are finite at $\theta=0$. As $\theta\to\pi$ ($T\to\infty$) it follows from [37] that

$$\left.\begin{aligned}&\eta\sim\frac{\mathrm{A}}{T^{\lambda-1}}+\frac{1}{\lambda-1},\quad \lambda\neq 1,\\ &\eta\sim\mathrm{B}+\log T,\quad \lambda=1,\end{aligned}\right\} \qquad [39]$$

where A and B are constants. Thus, as $\theta\to\pi$, we have

$$\left.\begin{aligned}&\eta,\ \frac{\mathrm{d}\eta}{\mathrm{d}\theta},\ \frac{\mathrm{d}\eta}{\mathrm{d}\theta}\sin\theta\to\infty \quad \text{if} \quad \lambda<1,\\ &\eta,\ \frac{\mathrm{d}\eta}{\mathrm{d}\theta}\to\infty,\frac{\mathrm{d}\eta}{\mathrm{d}\theta}\sin\theta\to\text{const} \quad \text{if} \quad \lambda=1,\\ &\eta\to\frac{1}{\lambda-1},\ \frac{\mathrm{d}\eta}{\mathrm{d}\theta}\to\infty,\frac{\mathrm{d}\eta}{\mathrm{d}\theta}\sin\theta\to 0 \quad \text{if} \quad 1<\lambda<2,\\ &\eta\to\frac{1}{\lambda-1},\ \frac{\mathrm{d}\eta}{\mathrm{d}\theta}\to\text{const},\frac{\mathrm{d}\eta}{\mathrm{d}\theta}\sin\theta\to 0 \quad \text{if} \quad \lambda=2,\\ &\eta\to\frac{1}{\lambda-1},\ \frac{\mathrm{d}\eta}{\mathrm{d}\theta},\frac{\mathrm{d}\eta}{\mathrm{d}\theta}\sin\theta\to 0 \quad \text{if} \quad \lambda>2.\end{aligned}\right\} \qquad [40]$$

It is therefore clear that only if $\lambda>1$ can arguments similar to those described above be used to determine h_{π} from [30], whereas h_0 can be determined from [28] for all (positive) values of λ. In addition, it is clear that unless $\lambda>2$, $\mathrm{d}h/\mathrm{d}\theta$ will be non-zero as $\theta\to\pi$ and then spikes will occur in the film thickness at the bottom of the tube. It is worth noting that a typical solution to the unsimplified [26], shown in figure 2, appears to correspond to solutions of the simplified equation with $1<\lambda<2$.

The parameter λ is associated with the entrainment process and so a simple physical interpretation of the above results is that spikes will occur at the tube bottom unless the rate of entrainment is large enough to remove the liquid draining down the tube walls. Alternatively, it

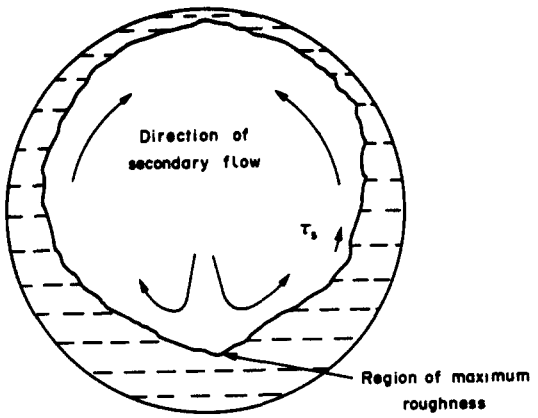

Figure 3. The secondary flow.

could be argued that liquid must drain sufficiently slowly to enable the entrainment process to remove the spikes. It should be noted, however, that even when conditions are such that smooth solutions at the tube bottom are obtained, they will not resemble those observed experimentally since, for $\lambda > 2$, we have

$$\left(\frac{\eta_\pi}{\eta_o}\right)_{max} = \left(\frac{h_\pi}{h_0}\right)^3_{max} = 3, \qquad [41]$$

i.e. $(h_\pi/h_0)_{max} = \sqrt[3]{3}$, which is far smaller than experimentally observed values, which are typically of order of magnitude 10 (Butterworth 1972).

The analysis of the equation governing film thickness has, therefore, explained why spikes can occur in the solution but does not explain observed experimental results for (h_π/h_0). We now look at two improvements to the model and assess their influence on this ratio.

2.3. The Effect of Non-zero Interfacial Shear Stress

It is well known that in turbulent flow over surfaces of unequal roughness secondary flows can be set up in a direction such that "turbulence rich" fluid is transported into regions of lower turbulence intensity (Hinze 1967). If we consider the liquid film to be a surface whose roughness increases with height then it follows that a secondary flow may be set up in the cross-section of the tube, in the direction shown in figure 3, giving rise to a non-zero interfacial shear stress τ_s. Laurinat *et al.* (1985) quote the experimental work of Darling & McManus (1967) in support of the assumption that τ_s is proportional to the product of mean axial interfacial shear stress and sin θ. In this work, for mathematical convenience, we assume that

$$\tau_s = -\beta h \sin\theta, \qquad [42]$$

where β is a constant. It is acknowledged that the above expression may not be capable of accurately representing the variation of circumferential shear stress with θ but it should be sufficiently accurate to enable useful qualitative conclusions to be drawn about the influence of this mechanism. Substitution of this expression into [24], again assuming a parabolic profile for u, leads to

$$\bar{u} = \frac{h^2 \sin\theta}{3\mu_T}\left(\rho g - \frac{3\beta}{2}\right), \qquad [43]$$

and the corresponding equation for h is

$$\frac{d}{d\theta}(h^3 \sin\theta) = \frac{3\mu_T R(D-E)}{\rho\left(\rho g - \frac{3\beta}{2}\right)}. \qquad [44]$$

It is unlikely that τ_s will be large enough to support the film and so $3\beta/2$ will be less than ρg. Comparison of the r.h.s. of [44] and [26] shows that the effect of allowing for non-zero τ_s is

qualitatively similar to that of increasing μ_T, and this could lead to slower draining of the film and a smooth solution for $\eta(\theta)$ at $\theta = \pi$. However, the maximum value of the ratio h_π/h_0 that could be obtained from the solution of [44] will still be too small.

2.4. The Effect of Varying Deposition Rate

In horizontal annular two-phase flow it is likely that the deposition rate D is not constant but varies with θ because the entrainment rate varies with θ and gravity will tend to enhance deposition near the tube bottom. Anderson & Russell (1970) and Hutchinson *et al.* (1974) have looked at some of the consequences of a variable deposition rate and the important result for the present analysis is that D increases as θ increases from 0 to π. The qualitative effect of varying D can be assessed via the simplified [31] but with

$$D = D^*\left[1 + \gamma \sin\left(\frac{\theta}{2}\right)\right], \tag{45}$$

where D^* replaces the previously constant D. In [45] D^* and γ are constants and the form of the expression for D is chosen because it is mathematically convenient and gives a deposition rate which increases from $\theta = 0$ to $\theta = \pi$. The solution for $\eta(\theta)$ now becomes

$$\eta(\theta) = \frac{1}{\sin\theta \tan^\lambda\left(\frac{\theta}{2}\right)} \int_0^\theta \left[1 + \gamma \sin\left(\frac{t}{2}\right)\right] \tan^\lambda\left(\frac{t}{2}\right) dt, \tag{46}$$

and has the same behaviour with λ as before as far as the appearance of spikes is concerned. However, if $\lambda > 1$ we now have

$$\left(\frac{h_\pi}{h_0}\right)_{\max} = \left(\frac{\eta_\pi}{\eta_0}\right)^{1/3}_{\max} = [3(1+\gamma)]^{1/3}, \tag{47}$$

and so for sufficiently large values of γ, i.e. a sufficiently rapidly varying deposition rate, it might be possible to obtain smooth solutions for the film thickness distribution which give experimentally observed values of h_π/h_0. Thus, in section 3 we develop a model for variable deposition rate and compare its predictions with experiments. Before doing so, however, we comment briefly on another approach that has been attempted to overcome the problem of film thickness spikes.

2.5. The Effect of Inertia Terms

In section 2.1 the circumferential flow problem was simplified by assuming $\delta/L \sim \mathrm{Re}^{-1} \ll 1$ and it was seen that this could lead to solutions in which the film thickness increased rapidly near $\theta = \pi$. Under these circumstances the approximations are not self-consistent and so we now look at two different estimates for the parameter δ/L.

2.5.1. $Re \gg 1$, $\delta/L \sim Re^{-1/2}$

The above conditions would only hold near $\theta = \pi$ and the momentum equations [8] and [9] would then be, in dimensional variables,

$$\rho\left(u\frac{\partial u}{\partial x} + v\frac{\partial u}{\partial y}\right) = -\frac{\partial p}{\partial x} + \frac{\partial \tau}{\partial y} + \rho g \sin\theta \tag{48}$$

and

$$0 = \frac{\partial p}{\partial y} + \rho g \sin\theta. \tag{49}$$

These equations can be manipulated in the same way as [15]–[17] with boundary conditions [18]–[20] and the assumptions that $\tau_s = 0$, u is parabolic and p_s is constant. The following equations for h and $\bar{u}$ result:

$$\frac{dh}{d\theta} = \frac{\dfrac{3\mu_T R\bar{u}}{h\rho} - ghR\sin\theta + \dfrac{\Gamma^* R\bar{u}(D-E)}{\rho}}{\Gamma\bar{u}^2 + gh\cos\theta} \tag{50}$$

and

$$\frac{d\bar{u}}{d\theta} = \frac{\dfrac{R(D-E)}{\rho} - \bar{u}\dfrac{dh}{d\theta}}{h}, \qquad [51]$$

where

$$\Gamma^* = 2\Gamma - \frac{3}{2} \qquad [52]$$

and

$$\Gamma = \frac{1}{h\bar{u}^2}\int_0^h u^2\,dy = \frac{6}{5}. \qquad [53]$$

The boundary conditions for [50] and [51] are

$$\bar{u} = 0 \quad \text{at} \quad \theta = 0 \quad \text{and} \quad \theta = \pi. \qquad [54]$$

Satisfactory solutions to the problem posed by [50], [51] and [54] have not been found. However, it is felt that the improvement to the model, due to the inclusion of inertia terms, will not be as great as that due to the inclusion of a variable deposition rate, for the following reason. The scaling required for the equations to hold is only valid near $\theta = \pi$, and so the inclusion of inertia terms will only influence the solution in that region. A variable deposition rate will influence the solution right around the circumference.

2.5.2. $\delta/L \sim 1$

Another possible scaling is that, near $\theta = \pi$, $\delta/L \sim 1$. In this case the inertia terms in both the circumferential and radial equations have to be retained. The numerical solution of the resulting system of equations is likely to be more difficult than in section 2.5.1 and so no solutions have been attempted. In addition, it is necessary to model more accurately the effects on momentum transfer of droplet deposition and entrainment. For these reasons it is concluded that the major gains, if any, from the inclusion of inertia and pressure gradient terms are likely to come from the approach of section 2.5.1.

3. A MODEL FOR THE DROPLET DEPOSITION RATE

In his review of droplet mass transfer in annular two-phase flow Hewitt (1978) describes two mechanisms by which droplets in the gas core may deposit on the liquid film on the tube wall.

Firstly, the droplets may redeposit under the influence of a succession of interactions with gas phase turbulent eddies. A model for this process has been developed by Hutchinson *et al.* (1971) who show that the overall process may, under certain circumstances, be described by a diffusion equation. Hutchinson *et al.* (1974) have shown how to extend this model to horizontal annular flow but, for reasons to be given below, we do not pursue this approach here.

Secondly, the droplets may deposit as a direct result of the velocity they acquire on their ejection from the liquid film. Photographic evidence shows that this is the primary deposition mechanism for droplets with diameter greater than about 150 μm in vertical annular flow (Whalley *et al.* 1979).

The deposition process is, then, in general due to a combination of these two mechanisms. Chang (1973) argues that, in horizontal annular flow, the second mechanism is chiefly responsible for the deposition of droplets with diameter less than about 25 μm, whereas in the work of James *et al.* (1980) it is found that a good description of the unidirectional deposition data in vertical annular flow can be obtained if it is assumed that only about 30% of the droplets deposit via the second mechanism, the remaining 70% depositing via the diffusion mechanism. One explanation for this apparent discrepancy may be that in horizontal annular flow most of the droplets are entrained from the region near the bottom of the tube where the film is typically much thicker than those found in vertical annular flow. Consequently, the size of the droplets generated may be larger and the second deposition mechanism dominant. It should also be noted that Hutchinson *et al.* (1974) have shown that the effect of gravity on the diffusion mechanism is small, from which it

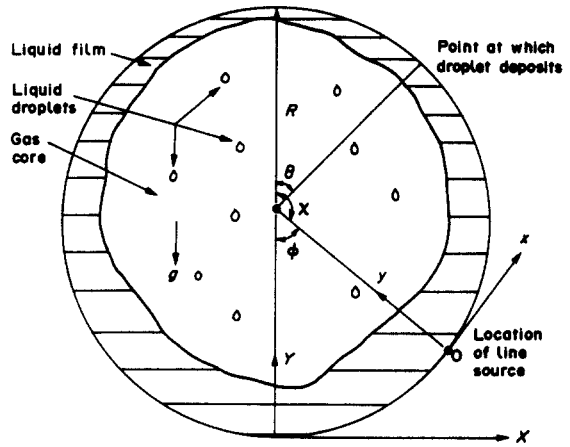

Figure 4. Definition sketch of horizontal annular flow showing the coordinates (X, Y) Oxy and x.

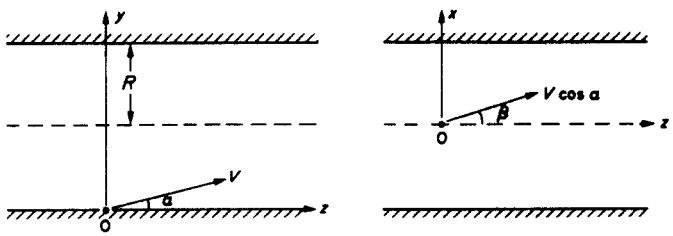

Figure 5. Definition sketch for ejection angles α and β.

may be inferred that the required variation of deposition flux around the circumference could not occur if diffusion was the dominant method of deposition. For these reasons we therefore proceed on the assumption that the sole mechanism responsible for deposition in horizontal annular flow is the second mechanism; thus the work that follows is an extension of that of Anderson & Russell (1970).

3.1. Mathematical Formulation

We assume that droplets are emitted from a continuous distribution of line sources around the tube periphery, follow a parabolic trajectory solely under the influence of gravity, and subsequently deposit on the tube wall at some downstream location. In reality the sources for droplet entrainment are at the tips of roll-waves which propagate along the film. However, to facilitate the analysis we neglect the film thickness, for the purposes of deriving an expression for variable deposition rate, and assume that the droplets originate and deposit at the tube wall. The notation θ will refer to the angular location of the point of deposition and χ (or $\phi = \pi - \chi$) to the location of the line source, as shown in figure 4.

From the symmetry of the problem about the line $\theta = 0, \pi$ it follows that if θ is allowed to vary over a range of length 2π, a range of length π need only be considered for χ. For every line source we assume that the droplets are emitted at the same speed V along trajectories which make angles α and β with the planes Oxz and Oyz, respectively, at the point of ejection (see figure 5).† While it is assumed that V is constant, the angles α and β are taken to be independent random variables distributed uniformly on $(0, \alpha_0)$, $(-\beta_0, \beta_0)$, respectively. The joint probability density function of α and β is therefore

$$p(\alpha, \beta) = \frac{1}{2\alpha_0\beta_0}, \quad \alpha \in (0, \alpha_0), \quad \beta \in (-\beta_0, \beta_0),$$
$$= 0, \text{ otherwise.} \qquad [55]$$

†Note that the coordinate direction x defined in section 3 is in the opposite direction to that defined in section 2. In addition, no confusion should arise over the use of the previously defined symbols β and V.

If the probability density function for deposition at θ from a line source at χ, $p(\theta;\chi)$ can be found and if the strength of the line source at χ, $E(\chi)$ is known, then the deposition rate at angle θ, $D(\theta)$ will be given by

$$D(\theta) = \int_0^{2\pi} E(\chi)\, p(\theta;\chi)\, d\chi = \int_0^{\pi} E(\chi)\,[p(\theta;\chi) + p(2\pi - \theta;\chi)]\, d\chi, \qquad [56]$$

from symmetry. The problem of specifying $D(\theta)$ therefore reduces to that of finding $p(\theta;\chi)$.

Since we are only interested in fully developed flow, the axial motion of the droplets need not be considered in detail and V may be taken to be approximately equal to the mean gas phase velocity. The only force acting on a droplet in the plane of the cross-section, Oxy, is gravity and so the position (X, Y) referred to cartesian axes fixed at the tube bottom, of a droplet ejected from a line source at $\chi = \pi - \phi$ after a time t is given by

$$X = R\sin\phi + Vt\cos\alpha\sin\beta\cos\phi - Vt\sin\alpha\sin\phi, \qquad [57]$$

$$Y = R(1-\cos\phi) + Vt\sin\alpha\cos\phi + Vt\sin\beta\cos\alpha\sin\phi - \frac{gt^2}{2}. \qquad [58]$$

Experimental evidence suggests that α_0 and β_0 are small enough to write

$$\sin\alpha \approx \alpha, \quad \cos\alpha \approx 1, \quad \sin\beta \approx \beta, \qquad [59]$$

and since, when a droplet reaches the boundary of the tube

$$X = R\sin\theta, \quad Y = R(1+\cos\theta), \qquad [60]$$

we have

$$R\sin\theta = R\sin\phi + V\beta t\cos\phi - V\alpha t\sin\phi,$$

$$R\cos\theta = -R\cos\phi + V\alpha t\cos\phi + V\beta t\sin\phi - \frac{gt^2}{2}. \qquad [61]$$

Hence

$$\alpha = \frac{R[1+\cos(\theta+\phi)]}{Vt} + \frac{\mu Vt\cos\phi}{R}$$

and

$$\beta = \frac{R\sin(\theta+\phi)}{Vt} + \frac{\mu Vt\sin\phi}{R}, \qquad [62]$$

where

$$\mu = \frac{gR}{2V^2}. \qquad [63]$$

The joint probability density function for deposition at θ at time t after ejection from $\chi(=\pi-\phi)$, $p(\theta, t;\chi)$, may now be found from

$$p(\theta, t;\chi) = |J|\, p(\alpha, \beta), \qquad [64]$$

where the Jacobian J is given by

$$J = \frac{\partial\alpha}{\partial\theta}\frac{\partial\beta}{\partial t} - \frac{\partial\beta}{\partial\theta}\frac{\partial\alpha}{\partial t} = \frac{R^2}{V^2t^3}[1+\cos(\theta+\phi)] - \frac{\mu\cos\theta}{t}. \qquad [65]$$

Thus

$$p(\theta, t;\chi) = \frac{1}{2\alpha_0\beta_0}\left\{\frac{R^2}{V^2t^3}[1+\cos(\theta+\phi)] - \frac{\mu\cos\theta}{t}\right\}, \qquad [66]$$

over some region of (θ, t) space.

3.2. The Limits in (θ, t) Space

The region of (θ, t) space over which $p(\theta, t; \chi)$ is non-zero is determined from two considerations. First, the fact that $p(\alpha, \beta)$ is zero outside the rectangle $0 < \alpha < \alpha_0, -\beta_0 < \beta < \beta_0$ leads to the following limits:

(i) $\alpha < \alpha_0$ requires

$$\frac{R}{2\mu V \cos\phi}\left\{\alpha_0 - \sqrt{\alpha_0^2 - 4\mu \cos\phi\,[1+\cos(\theta+\phi)]}\right\} < t$$
$$< \frac{R}{2\mu V \cos\phi}\left\{\alpha_0 + \sqrt{\alpha_0^2 - 4\mu \cos\phi\,[1+\cos(\theta+\phi)]}\right\} \quad [67]$$

if $\cos\phi > 0$, and

$$\frac{R}{2\mu V \cos\phi}\left\{\alpha_0 - \sqrt{\alpha_0^2 - 4\mu \cos\phi\,[1+\cos(\theta+\phi)]}\right\} < t \quad [68]$$

if $\cos\phi < 0$;

(ii) $\alpha > 0$ requires

$$t^2 < -\frac{R^2}{\mu V^2 \cos\phi}\,[1+\cos(\theta+\phi)] \quad [69]$$

if $\cos\phi < 0$;

and

(iii) $-\beta_0 < \beta < \beta_0$ requires

$$\frac{R}{2\mu V \sin\phi}\left[\beta_0 - \sqrt{\beta_0^2 - 4\mu \sin\phi \sin(\theta+\phi)}\right] < t$$
$$< \frac{R}{2\mu V \sin\phi}\left[\beta_0 + \sqrt{\beta_0^2 - 4\mu \sin\phi \sin(\theta+\phi)}\right]. \quad [70]$$

The above inequalities require

$$\sin\phi \sin(\theta+\phi) \leqslant \frac{\beta_0^2}{4\mu} \quad [71]$$

and

$$\cos\phi\,[1+\cos(\theta+\phi)] < \frac{\alpha_0^2}{4\mu};$$

for values of θ and ϕ which do not satisfy the above inequalities, $p(\theta, t; \chi)$ is zero.

The second set of restrictions stems from the fact that, while the elimination of θ from [61] leads to a cubic equation for t which may have three real roots (corresponding to droplet trajectories which cross the tube boundary twice†), the physical problem requires that a droplet never leaves the interior of the tube. At any time $s \in (0, t)$ the position of the droplet is

$$X = R\sin\phi + (V\beta\cos\phi - V\alpha\sin\phi)\,s, \quad [72]$$

$$Y = R(1-\cos\phi) + (V\alpha\cos\phi + V\beta\sin\phi)\,s - \frac{g s^2}{2}. \quad [73]$$

Elimination of α and β between [61], [72] and [73] gives

$$X = R\sin\phi + \frac{s}{t}R\,(\sin\theta - \sin\phi), \quad [74]$$

$$Y = R\,(1-\cos\phi) + \frac{s}{t}R\,(\cos\theta + \cos\phi) + \frac{g}{2}s(t-s). \quad [75]$$

†Chang (1973) implicitly assumes that the cubic has only one real root, which is not necessarily true.

The droplet will never leave the interior of the tube if

$$X^2 + (Y - R)^2 \leqslant R^2 \quad \forall s \in (0, t), \tag{76}$$

which leads to

$$\mu^2 V^4 t^2 s^2 - s\,[2\mu V^2 R^2 t\,(\cos\theta + \cos\phi) + \mu^2 V^4 t^3] + 2R^4[1 + \cos(\theta + \phi)] + 2\mu V^2 R^2 t^2 \cos\phi \geqslant 0 \quad \forall s \in (0, t). \tag{77}$$

The restrictions on t, given θ and ϕ, that emerge from this equation are given below, but, because of its complexity, their derivation is given in appendix A:

(i) for $\cos\phi > 0$ we require

$$t^2 < \frac{4R^2}{\mu V^2} \sin\frac{\phi - \theta}{2}\left(1 - \sin\frac{\theta + \phi}{2}\right), \quad \theta \in \left(-\pi - \phi, -\frac{\pi - \phi}{3}\right), \tag{78}$$

$$t^2 < \frac{R^2}{\mu V^2} \frac{1 + \cos(\theta + \phi)}{\cos\theta}, \quad \theta \in \left(-\frac{\pi - \phi}{3}, \frac{\pi + \phi}{3}\right), \tag{79}$$

$$t^2 < \frac{4R^2}{\mu V^2} \sin\frac{\theta - \phi}{2}\left(1 + \sin\frac{\theta + \phi}{2}\right), \quad \theta \in \left(\frac{\pi + \phi}{3}, \pi - \phi\right); \tag{80}$$

and

(ii) for $\cos\phi < 0$ we require

$$t^2 < -\frac{R^2}{\mu V^2} \frac{[1 + \cos(\theta + \phi)]}{\cos\phi}, \quad \theta \in (-2\pi + \phi, 3\phi - 3\pi) \text{ and } \theta \in (\pi - \phi, \phi), \tag{81}$$

$$t^2 < \frac{4R^2}{\mu V^2} \sin\frac{(\phi - \theta)}{2}\left(1 - \sin\frac{\theta + \phi}{2}\right), \quad \theta \in \left(3\phi - 3\pi, -\frac{\pi - \phi}{3}\right) \tag{82}$$

$$t^2 < \frac{R^2}{\mu V^2} \frac{1 + \cos(\theta + \phi)}{\cos\theta}, \quad \theta \in \left(-\frac{\pi - \phi}{3}, \pi - \phi\right). \tag{83}$$

The probability density function $p(\theta; \chi)$ is now given by

$$p(\theta; \chi) = \int_{T_L}^{T_U} p(\theta, t; \chi)\,\mathrm{d}t = \frac{1}{2\alpha_0\beta_0}\left\{-\frac{R^2[1 + \cos(\theta + \phi)]}{2V^2 t^2} - \mu\cos\theta \log t\right\}_{T_L}^{T_U}, \tag{84}$$

where T_U and T_L are the appropriate upper and lower limits for t. In section 4 we shall require the mean time of flight of particles ejected from a line source at χ, $\bar{t}(\chi)$, and this is given by

$$\bar{t}(\chi) = \int_\theta \int_{T_L}^{T_U} t\,p(\theta, t; \chi)\,\mathrm{d}t\,\mathrm{d}\theta = \frac{1}{2\alpha_0\beta_0} \int_\theta \left\{-R^2 \frac{[1 + \cos(\theta + \phi)]}{V^2 t} - \mu\cos\theta t\right\}_{T_L}^{T_U} \mathrm{d}\theta, \tag{85}$$

where the range of θ is $(-\pi - \phi, \pi - \phi)$ for $\cos\phi > 0$ or $(-2\pi + \phi, \phi)$ for $\cos\phi < 0$.

3.3. The Probability Density Function $p(\theta; \chi)$

In this section some of the properties of $p(\theta, \chi)$ are illustrated by means of examples. In figures 6–10 we plot $p(\theta; \chi)$ for $\chi = 0°$, 30°, 90°, 120° and 180° with $\alpha_0 = \beta_0 = 1.5°$ and $\mu = 2.65 \times 10^{-5}$ (these figures correspond to a gas velocity $V = 54.4$ m/s, and tube radius $R = 16$ mm) and the following features can be seen. There is a peak in the probability density function at $\pm 90°$ from the location of the source and, when the source is in the lower half of the tube, there is a singularity at the source itself. This singularity occurs because the upper limit for t, given by [80], is non-zero whereas the lower limit, given by [67], [68] or [70] is zero. There is then a logarithmic singularity in $p(\theta; \chi)$, as can be seen from [84]. In figure 11 we see that the effect of unequal α_0 and β_0 is to remove the peak at $-90°$ from the source and to change the overall shape of the probability density function (cf. figure 6).

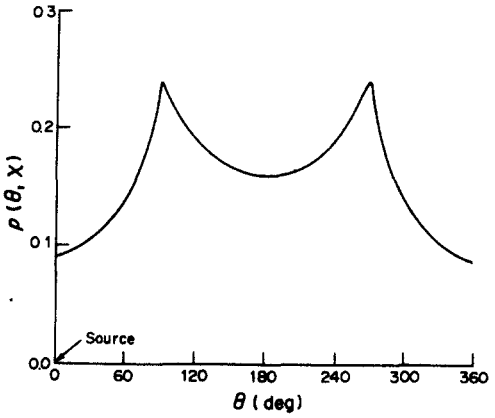

Figure 6. The probability density function for a source at $\chi = 0°$ ($\alpha_0 = \beta_0 = 1.5°$, $\mu = 2.65 \times 10^{-5}$).

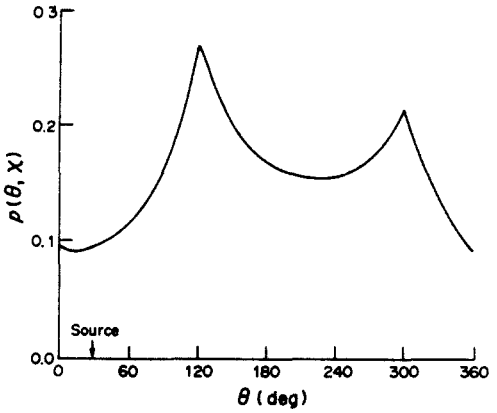

Figure 7. The probability density function for a source at $\chi = 30°$ ($\alpha_0 = \beta_0 = 1.5°$, $\mu = 2.65 \times 10^{-5}$).

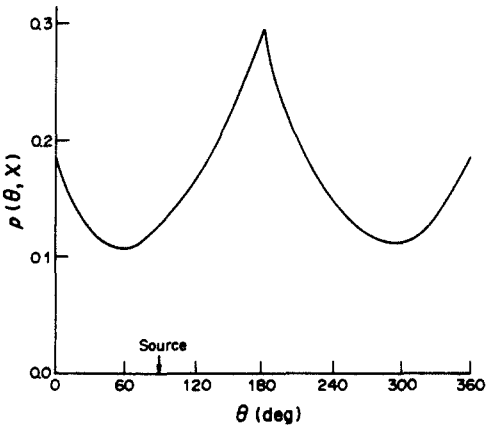

Figure 8. The probability density function for a source at $\chi = 90°$ ($\alpha_0 = \beta_0 = 1.5°$, $\mu = 2.65 \times 10^{-5}$).

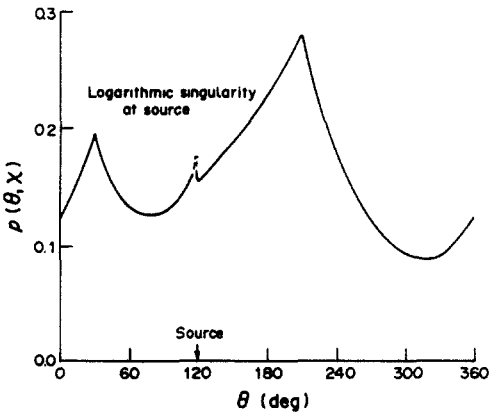

Figure 9. The probability density function for a source at $\chi = 120°$ ($\alpha_0 = \beta_0 = 1.5°$, $\mu = 2.65 \times 10^{-5}$).

In figure 12 we plot $p(\theta; \chi)$ for $\chi = 180°$ with $\alpha_0 = \beta_0 = 1.5°$ but $\mu = 2.65 \times 10^{-7}$, i.e. reduced by a factor of 100. This approximates the zero-gravity case and therefore the plot of $p(\theta; \chi)$ with $\chi = 0$ should be the same, as indeed it is. When $\mu = 0$, it is possible to obtain the exact results

$$p(\theta) = \frac{\alpha_0}{4\beta_0} \frac{1}{1 + \cos\theta}, \quad \theta \in (0, \theta^*), \quad \theta \in (2\pi - \theta^*, 2\pi),$$
$$= \frac{\beta_0}{4\alpha_0} \frac{1}{1 - \cos\theta}, \quad \theta \in (\theta^*, 2\pi - \theta^*), \qquad [86]$$

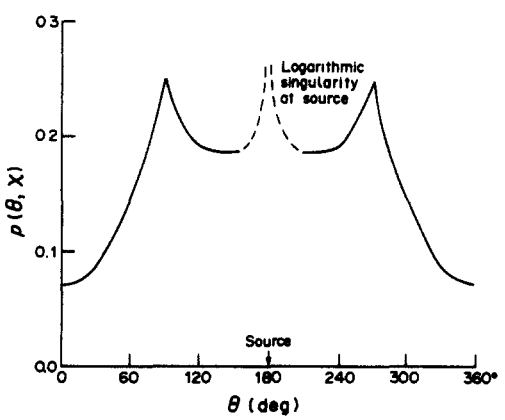

Figure 10. The probability density function for a source at $\chi = 180°$ ($\alpha_0 = \beta_0 = 1.5°$, $\mu = 2.65 \times 10^{-5}$).

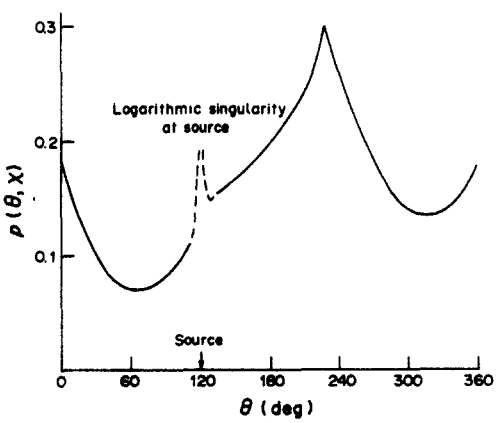

Figure 11. The probability density function for a source at $\chi = 120°$ ($\alpha_0 = 1.5°$, $\beta_0 = 1°$, $\mu = 2.65 \times 10^{-5}$).

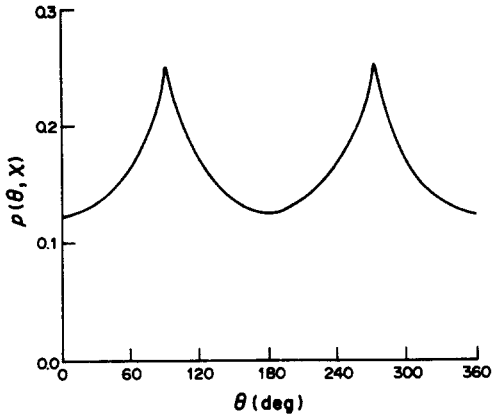

Figure 12. The probability density function for a source at $\chi = 180°$ or $X = 0°$ ($\alpha_0 = \beta_0 = 1.5°$, $\mu = 2.65 \times 10^{-7}$).

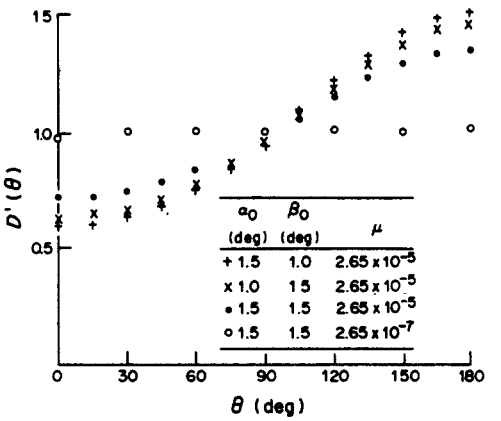

Figure 13. Reduced deposition $D'(\theta)$ for various α_0, β_0 and μ.

where

$$\theta^* = \tan^{-1}\frac{\beta_0}{\alpha_0}, \qquad [87]$$

and it is readily seen that this expression closely approximates the curve shown in figure 12 when $\alpha_0 = \beta_0$. A check on the results so far is that

$$\int_0^{2\pi} p(\theta;\chi)\,d\theta = 1, \qquad [88]$$

for all χ and a numerical integration confirms that this is the case for all the examples above (indeed, a quick check can be obtained by noting that if $p(\theta;\chi)$ were constant then it must take the value $1/2\pi = 0.16$ approx., and all the curves illustrated are distributed around this value). Finally, in figure 13 we illustrate a reduced deposition rate $D'(\theta)$, defined by

$$D'(\theta) = \int_0^{\pi} [p(\theta;\chi) + p(2\pi - \theta;\chi)]\,d\chi, \qquad [89]$$

for different values of α_0, β_0 and μ as shown. It is seen that the theory predicts the 'S'-shaped curve observed experimentally (Anderson & Russell 1970; Chang 1973) and that the effect of reducing μ (i.e. gravity) is to produce a constant value of $D' \approx 1$, which is what we expect.

4. THE EFFECT OF VARIABLE DEPOSITION RATE $D(\theta)$

The results of the last section are now incorporated into the circumferential flow model, given by [26], but with $D(\theta)$ replacing the previously constant D. The scaling factor H^3, defined by [33] is now redefined as

$$H^3 = \frac{3\mu_T R E_0}{\rho^2 g}, \qquad [90]$$

where E_0 is a constant with the dimensions of entrainment flux, and we introduce a non-dimensional film thickness $\eta(\theta)$ as before, [32]. Finally, if we again assume that the non-dimensional entrainment rate may be written as a constant, λ, times $\eta(\theta)$ then we arrive at the following equation for $\eta(\theta)$:

$$\frac{d}{d\theta}[\eta(\theta)\sin\theta] + \lambda\eta(\theta) = \lambda \int_0^{2\pi} p(\theta;\chi)\,\eta(\chi)\,d\chi. \qquad [91]$$

This assumption is not essential for the solution of [91] but it does allow an estimate of λ to be made (from the analysis of section 2) for which acceptably smooth solutions exist. The assumption

is equivalent to $E(h) \propto h^3$, which is not unreasonable. In fact Fisher & Pearce (1978) show that the correlation of Hutchinson & Whalley (1973) may be written in the form $E(h) \propto h^2 \times$ (axial shear stress)^2 and so, if the axial shear stress increases as $\sqrt{h}$, the assumption is valid. However, it is not claimed that the assumption *is* exact but merely that it is reasonable; the parameter λ is estimated from the analysis of section 2, not from experimental data.

Equation [91] is a linear integro-differential equation which is homogeneous in $\eta(\theta)$ and so we apply the (arbitrary) boundary condition

$$\eta(0) = 1. \qquad [92]$$

The proof that non-zero solutions for $\eta(\theta)$ exist and are unique is given in appendix B and details of the numerical scheme employed to solve [91] are given in appendix C.

The model now contains five "free" parameters; λ, α_0, β_0 and any two of μ_T, H^3 and E_0. The requirement that global mass balance must be satisfied, i.e. the requirement that the sum of entrained liquid and liquid flowing axially in the film must equal the known total mass flux, will effectively reduce this number to four. In section 2 it was shown that when $D(\theta)$ is constant, [31] has solutions for $\eta(\theta)$ with no spikes at $\theta = \pi$ only if $\lambda > 2$. A similar restriction appears to hold for [91] and so we fix $\lambda = 2.2$. Higher values of λ could be used and will result in solutions for $\eta(\theta)$ with no spikes at $\theta = \pi$. However, the profile $h(\theta)$ is not very sensitive to values of λ in the range 2–3 and the smaller we can make λ, consistent with physically acceptable solutions, the better the agreement with experiment, as discussed in section 4.3.

We are now left with three parameters α_0, β_0 and μ_T, say, to specify before predictions of film thickness and film flowrate distributions can be made and appeal to a result from vertical annular flow to reduce this number to two.

4.1. Restrictions on α_0 and β_0 from Vertical Annular Flow

In the case of vertical annular flow, in which gravity does not affect droplet trajectories in the plane of the tube cross-section, and there is axial symmetry, the mean time of flight $\bar{t}(\chi)$ will be independent of χ. From [61], after eliminating θ and setting $\mu = 0$, we find

$$t = \frac{2\alpha R}{V(\alpha^2 + \beta^2)}. \qquad [93]$$

The mean time of flight, $\bar{t}$, is therefore independent of χ and is given by

$$\bar{t} = \int_0^{\alpha_0} \int_{-\beta_0}^{\beta_0} t(\alpha, \beta)\, p(\alpha, \beta)\, \mathrm{d}\beta\, \mathrm{d}\alpha = \frac{R}{V \alpha_0 \beta_0}\left[\beta_0 \log\left(1 + \frac{\alpha_0^2}{\beta_0^2}\right) + 2\alpha_0 \tan^{-1}\frac{\beta_0}{\alpha_0}\right]. \qquad [94]$$

In fully developed vertical annular flow the concentration of droplets in the gas core, C, may be related to the (constant) entrainment rate E, and $\bar{t}$, as

$$C = \frac{2}{R} E \bar{t}. \qquad [95]$$

Whalley *et al.* (1974) show that in fully developed vertical annular flow it is possible to relate E to C via a constant, k, known as the mass transfer coefficient, as follows:

$$E = k C. \qquad [96]$$

Equations [94]–[96] can now be combined to give

$$\beta_0 \log\left(1 + \frac{\alpha_0^2}{\beta_0^2}\right) + 2\alpha_0 \tan^{-1}\left(\frac{\beta_0}{\alpha_0}\right) = \frac{V \alpha_0 \beta_0}{2k}. \qquad [97]$$

In a given flow V and k will be known ($k = 0.15$ m/s for an air–water system at atmospheric pressure) and so β_0 can be predicted in terms of α_0.

Although the above relationship between α_0 and β_0 has been derived from a consideration of vertical annular flow, we assume that since the mechanisms by which droplets are ejected into the gas stream are similar in horizontal and vertical annular flows, the relationship holds for horizontal annular flows also.

4.2. Further Assumptions and the Solution Procedure

Two further relationships will now be proposed which enable predictions of the film thickness and film flowrate to be made.

Firstly, we assume that the rate of entrainment at the top of the tube ($\theta = 0$) is the same as that which would be predicted from the correlation of Hutchinson & Whalley (1973) for a vertical annular flow with the same film thickness and shear stress as that which occurs at the top of the tube. This assumption is reasonable because the observed film thickness distributions near the top of the tube do not vary very much around the circumference and are of similar magnitude to those found in vertical annular flows. The assumption would not be valid near the tube bottom ($\theta = \pi$) where the film thickness varies rapidly around the circumference and is typically larger than those on which the correlation of Hutchinson & Whalley (1973) is based. Fisher & Pearce (1978) point out that a reasonable approximation to the correlation of Hutchinson & Whalley (1973) is

$$E(\theta) = \frac{52.2\,\tau_A^2(\theta)\,h^2(\theta)}{\sigma^2}\ \text{kg/m}^2\,\text{s}, \qquad [98]$$

where $\tau_A(\theta)$ is the (axial) interfacial shear stress at location θ and σ is the surface tension. Fisher & Pearce (1978) also give a correlation for $\tau_A(\theta)$ in terms of $h(\theta)$, strictly only valid for tubes of 31.8 mm i.d., and it is this correlation which is used in the present work (see below). The above assumption leads to the equation

$$E(0) = \lambda E_0, \qquad [99]$$

when it is noted that $\eta(0) = 1$.

The second, and final, relationship required for the solution of [91] is obtained from the assumption that the average ejection velocity of droplets along the radius (direction Oy in figure 5) is proportional to the local turbulent intensity at the point of ejection. Taking the average ejection velocity to be approximately equal to $V\alpha_0$, we may therefore write

$$\alpha_0 = \frac{K\,u^*}{V}, \qquad [100]$$

where u^* is the friction velocity at the interface, defined by

$$u^* = \sqrt{\frac{\tau_A(\theta)}{\rho_G}}, \qquad [101]$$

and K is a constant which we expect to be of order of magnitude 1. The interfacial shear stress is found from the correlation of Fisher & Pearce (1978):

$$\tau_A(\theta) = \tau_0\left[1 + \frac{90\,h(\theta)}{R}\right], h(\theta) \leqslant 280\,\mu\text{m}$$

$$= 2.6\,\tau_0, h(\theta) > 280\,\mu\text{m}, \qquad [102]$$

where τ_0 is the wall shear stress defined by

$$\tau_0 = \tfrac{1}{2}\rho_{GC}\,V_{GC}^2 f_{GC}, \qquad [103]$$

ρ_{GC} is the gas core density defined by

$$\rho_{GC} = \rho_G + C, \qquad [104]$$

V_{GC} is the gas core velocity defined by

$$V_{GC} = \frac{G_{LE}}{C}, \qquad [105]$$

where G_{LE} is the entrained liquid mass flux, and f_{GC} is the gas core friction factor defined by

$$f_{GC} = 0.079\,\text{Re}_{GC}^{-1/4}, \qquad [106]$$

where

$$\text{Re}_{GC} = \frac{2\,V_{GC}R}{\mu_G}\rho_{GC}, \qquad [107]$$

μ_G being the gas dynamic viscosity. Pearce (1977) arrives at the above correlation by taking G_{LE} to be one half of the total liquid mass flux G_L. We shall use this correlation for $\tau_A(\theta)$ in the calculations described below but for simplicity in the calculation of α_0, which we have implicitly assumed does not depend on θ, we take $\tau_A(\theta)$ to be constant in [101] and equal to $\frac{1}{2}\rho_G V^2 f_{GC}$. This leads to

$$\alpha_0 = K\sqrt{\frac{f_{GC}}{2}}. \qquad [108]$$

The constant K is estimated from the experiments of Whalley *et al.* (1979) to be about 0.57.

The calculation of film thickness and film flowrate distributions can now be carried out via the following steps:

(i) given the physical properties, tube radius and liquid and gas mass fluxes, calculate α_0 as described above;
(ii) calculate β_0 from the vertical flow constraint given by [97];
(iii) with $\lambda = 2.2$ solve [91] for $\eta(\theta)$;
(iv) compute $\bar{t}(\chi)$ from [85];
(v) guess a value of G_{LE};
(vi) compute E_0 from the relationship

$$\lambda E_0 \int_0^{2\pi} \bar{t}(\chi)\,\eta(\chi)\,d\chi = C; \qquad [109]$$

(vii) evaluate $H^3 = h^3$ $(\theta = 0)$ from the first of the assumptions described in this section, and hence obtain the profile $h(\theta)$;
(viii) evaluate the local axial film flowrate $\Gamma_A(\theta)$, defined by

$$\Gamma_A(\theta) = \rho_L \int_0^{h(\theta)} U(y,\theta)\,dy, \qquad [110]$$

where $U(y,\theta)$ is the local axial liquid velocity,† and hence obtain the liquid film mass flux, G_{LF}, from

$$G_{LF} = \frac{1}{\pi R}\int_0^{2\pi} \Gamma_A(\theta)\,d\theta; \qquad [111]$$

(ix) obtain a new estimate of G_{LE} from global mass balance, $G_{LF} + G_{LE} = G_L$, where G_L is the (known) total liquid mass flux, return to step (vi) and iterate to convergence.

4.3. Comparison with Experimental Data

In figures 14–17 the predicted and experimentally measured film thicknesses are compared. The data are those of Butterworth (1972) and Butterworth & Pulling (1974) who carried out experiments with air and water in 31.8 mm i.d. horizontal tubes. The physical properties for these runs were taken to be μ_L (the liquid dynamic viscosity) $= 10^{-3}$ N/ms, $\mu_G = 1.81 \times 10^{-5}$ N/ms, $\rho = 10^3$ kg/m^3, $\sigma = 72 \times 10^{-3}$ N/m and $g = 9.81$ m/s^2.

The gas density, liquid mass flux and gas mass flux for each run are given in the figures. It can be seen that the predictions are generally in good agreement with the experimental data for maximum and minimum film thickness and, moreover, the variation of h with θ is similar to that observed. Calculated values of α_0 and β_0 are also given and are of the order of magnitude we would expect. The calculated entrained liquid mass fluxes are also given and it is seen that while they are in reasonable agreement with experiment, they are consistently high. Since it is extremely difficult to obtain accurate measurements of the entrained liquid mass flux and in view of the approximations employed in the model for entrainment flux, these comparisons do not provide strong evidence for or against the model. Nevertheless, since the entrained liquid mass flux depends on λ, the above comparison suggests that this parameter should be chosen to be as small as possible, subject to the constraint that physically acceptable solutions to the model equations are obtained.

†We assume that the well-known logarithmic wall velocity profile may be applied locally at θ.

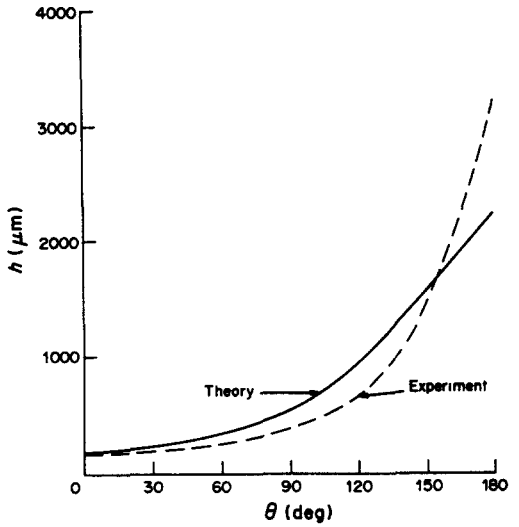

Figure 14. Comparison of theoretical and experimental film thickness profiles. Butterworth (1972) data: $G_L = 159$ kg/m^2 s, $\rho_G = 1.7$ kg/m^3, $G_G = 32$ kg/m^2 s, G_{LE} (theory) = 15.1 kg/m^2 s, G_{LE} (exp) $\simeq$ 9 kg/m^2 s, $\alpha_0 = 1.4°$, $\beta_0 = 2.4°$.

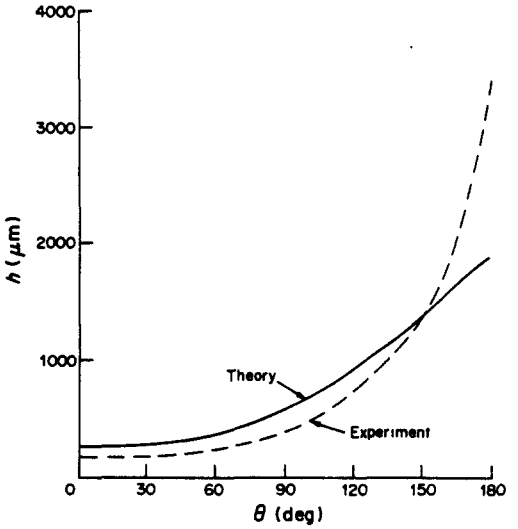

Figure 15. Comparison of theoretical and experimental film thickness profiles. Butterworth (1972) data: $G_L = 317$ kg/m^2 s, $G_G = 63.5$ kg/m^2 s, $\rho_G = 2.64$ kg/m^3, G_{LE} (theory) = 100 kg/m^2 s, G_{LE} (exp.) $\simeq$ 70 kg/m^2 s, $\alpha_0 = 1.3°$, $\beta_0 = 1.8°$.

Figures 18 and 19 show similar comparisons for the data of Fisher & Pearce (1978) and it is again seen that the model produces reasonable film thickness profiles. In figures 18 and 19 we have also shown the predictions obtained by Fisher & Pearce (1978) and, although it could be argued that they predict the maximum and minimum film thicknesses quite well, the present model accounts for the variation of h with θ more correctly. It is seen from figures 18 and 19 that the model predicts a more uniform film thickness distribution than that of Fisher & Pearce (1978).

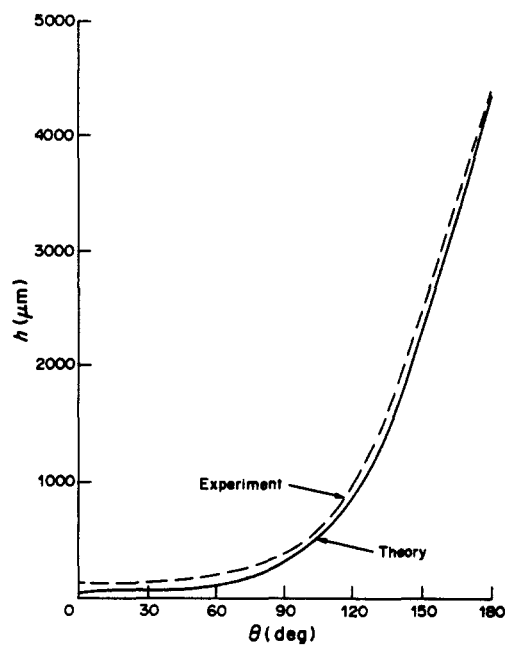

Figure 16. Comparison of theoretical and experimental film thickness profiles. Butterworth & Pulling (1974) data: $G_L = 161$ kg/m^2 s, $G_G = 31.5$ kg/m^2 s, $\rho_G = 3.0$ kg/m^3, G_{LE} (theory) = 24 kg/m^2 s, G_{LE} (exp.) $\simeq$ 12 kg/m^2 s, $\alpha_0 = 1.4°$, $\beta_0 = 4.7°$.

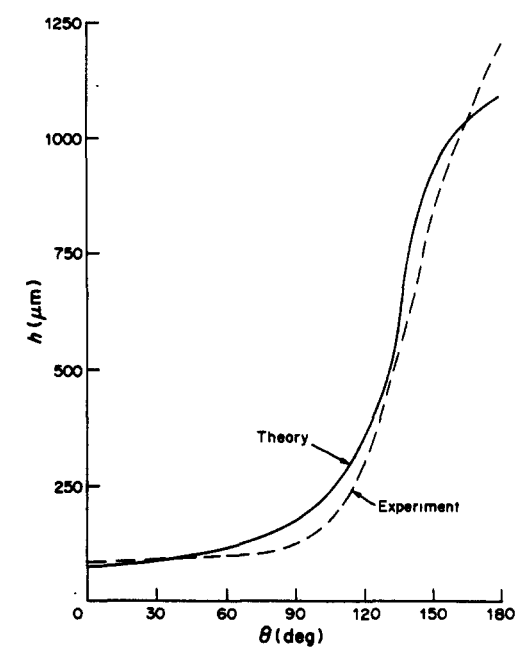

Figure 17. Comparison of theoretical and experimental film thickness profiles. Butterworth & Pulling (1974) data: $G_L = 81$ kg/m^2 s, $G_G = 64$ kg/m^2 s, $\rho_G = 3.0$ kg/m^2 s, G_{LE} (theory) = 5.0 kg/m^2 s, G_{LE} (exp.) $\simeq$ 2.0 kg/m^2 s, $\alpha_0 = 1.4°$, $\beta_0 = 2.0°$.

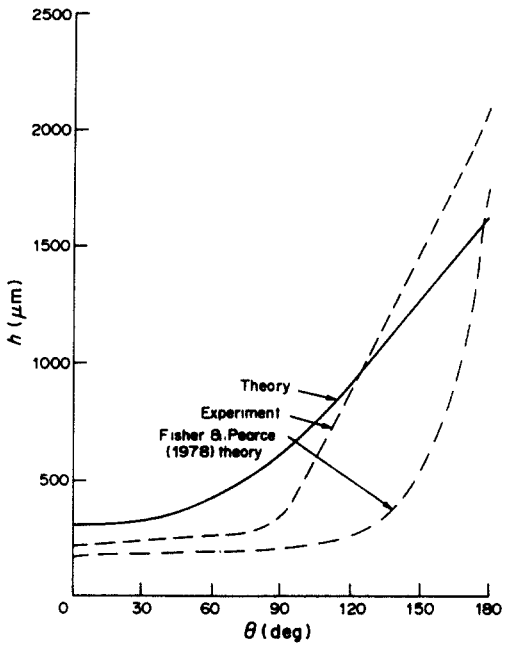

Figure 18. Comparison of theoretical and experimental film thickness profiles. Fisher & Pearce (1978) data: $G_L = 250\ kg/m^2\ s$, $G_G = 33\ kg/m^2\ s$, $\rho_G \simeq 1.25\ kg/m^2\ s$, G_{LE} (theory) $= 62\ kg/m^2\ s$, $\alpha_0 = 1.35°$, $\beta_0 = 1.5°$.

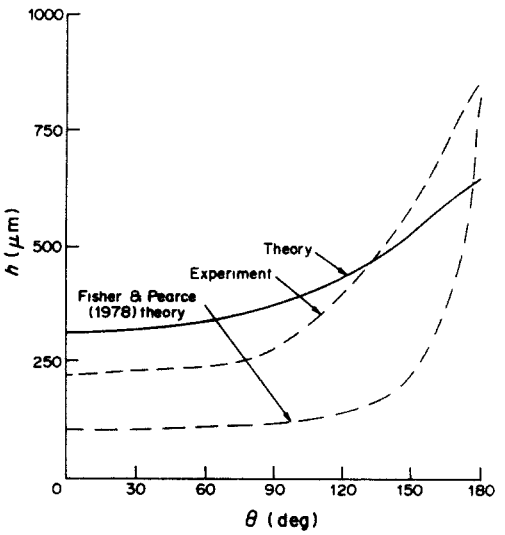

Figure 19. Comparison of theoretical and experimental film thickness profiles. Fisher & Pearce (1978) data: $G_L = 130\ kg/m^2\ s$, $G_G = 60\ kg/m^2\ s$, $\rho_G = 1.25\ kg/m^3$, G_{LE} (theory) $= 21\ kg/m^2\ s$, $\alpha_0 = 1.4°$, $\beta_0 = 0.55°$.

Since these authors assume a uniform deposition rate whereas the present model uses a variable deposition rate, in which more liquid is deposited at the bottom of the tube, the results seem at first sight surprising. The explanation is that there are differences, other than those concerning the deposition process, between the two models. Differences in the predictions of the two models cannot, therefore, be attributed to differences in the deposition process alone. In particular, Fisher & Pearce (1978) evaluate the film thickness distribution in the lower half of the tube in a completely different way from the present model.

Finally, in figure 20 we compare the axial film flowrate distributions from the experiments of Fisher & Pearce (1978) with the predictions of the present model. The agreement between theory and experiment is rather poor and, since the prediction of film thickness is quite reasonable for this set of conditions (figure 19), the result is rather surprising. One possible explanation is that the assumed local axial velocity profile (in this work the usual logarithmic profile) is in error.

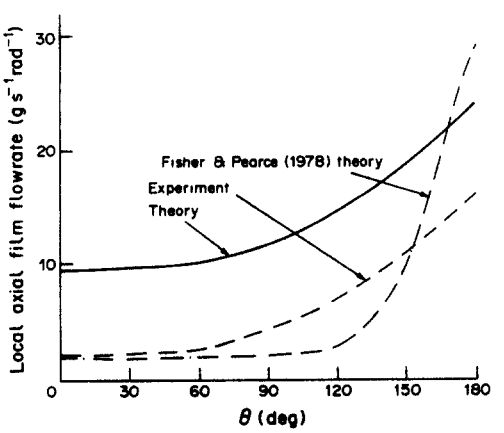

Figure 20. Comparison of theoretical and experimental film flowrates. Fisher & Pearce (1978) data: $G_L = 130\ kg/m^2\ s$, $G_G = 60\ kg/m^2\ s$, $\rho_G = 1.25\ kg/m^3$.

5. CONCLUSIONS

The major conclusions to be drawn from this work are as follows.

1. The governing equations for the circumferential flow are capable of producing acceptable solutions (i.e. solutions with no spikes at the tube bottom) if the rate of entrainment is sufficiently large (or, equivalently, the rate of liquid film drainage is small enough).
2. The inclusion of inertia terms and interfacial (circumferential) shear stress in the model are unlikely to significantly improve the agreement between theoretical and experimental values of the ratio (h_π/h_0) whereas the inclusion of a variable deposition rate is.
3. A model for the variable deposition rate, based on the assumption that droplets are ejected from the liquid film and execute a parabolic trajectory under the influence of gravity, shows at least qualitative agreement with observed experimental trends.
4. The incorporation of the model into the equations governing the circumferential flow enables reasonable predictions of the liquid film thickness distribution to be made.

Finally, it is appropriate to comment briefly on the model of Laurinat *et al.* (1985), who identify interfacial circumferential shear stress and normal Reynolds stress (which models oscillations in the circumferential film flow) as important mechanisms in horizontal annular flow, with the entrainment–deposition mechanism playing a secondary role. By adjusting the parameters which characterize the interfacial circumferential shear stress and normal Reynolds stress these authors obtain excellent agreement between theory and experiment. However, as stated by Laurinat *et al.* (1985), the relegation of the entrainment–deposition mechanism to a secondary role depends on the value taken for the mass-transfer coefficient characterizing the mechanism. In the present model, the value of the parameter characterizing this mechanism is large enough for smooth solutions for film thickness distributions to be obtained without the need for interfacial circumferential shear stress or normal Reynolds stresses. Lin *et al.* (1985) conclude that the deposition–entrainment process and interfacial circumferential shear stress are both important. We conclude that further improvements to the modelling of horizontal annular flow, and the establishment of the importance of the contributing mechanisms, can only take place when experimental data for the variation with θ of certain variables, notably entrainment flux, interfacial circumferential shear stress and mean axial velocity profiles, are available.

Acknowledgements—The authors would like to thank the referees for their constructive criticisms and for drawing our attention to the papers by Laurinat *et al.* (1985) and Lin *et al.* (1985).

REFERENCES

ANDERSON, R. J. & RUSSELL, T. W. F. 1970 Circumferential variation of interchange in horizontal annular two-phase flow. *Ind. Engng Chem. Fundam.* **9**, 340–344.

BUTTERWORTH, D. 1972 Air–water annular flow in a horizontal tube. *Prog. Heat Mass Transfer* **6**, 235–251.

BUTTERWORTH, D. & PULLING, D. J. 1974 Mechanisms in horizontal annular air–water flow. *Symp. on Multi-phase Flow Systems*, Univ. of Strathclyde, Glasgow, Paper A2.

CHANG, D. R. C. 1973 Generation, movement and deposition of droplets in annular two-phase flow. Ph.D. Thesis, Univ. of Delaware, Newark, Del.

DARLING, R. S. & MCMANUS, H. N. 1969 Flow patterns in circular ducts with circumferential variation of roughness: a two-phase analog. In *Developments in Mechanics*, Vol. 5 (Edited by WEISS H. J., YOUNG, D. F., RILEY, W. F. & ROGGE T. R.). Iowa State Univ. Press, Ames, Iowa.

FISHER, S. A. & PEARCE, D. L. 1978 A theoretical model for describing horizontal annular flows. Presented at *Int. Semin. on Momentum, Heat and Mass Transfer in Two-phase Energy and Chemical Systems*, Dubrovnik, Yugoslavia.

HEWITT, G. F. 1978 Liquid mass transport in annular two-phase flow. Presented at *Int. Semin. Momentum, Heat and Mass Transfer in Two-phase Energy and Chemical Systems*, Dubrovnik, Yugoslavia.

HINZE, J. O. 1967 Secondary currents in wall turbulence. *Phys. Fluids (Suppl.)* **10**, 112–125.

HUTCHINSON, P. & WHALLEY, P. B. 1973 A possible characterisation of entrainment in annular flow. *Chem. Engng Sci.* **28**, 974–975.

HUTCHINSON, P., HEWITT, G. F. & DUKLER, A. E. 1971 Deposition of liquid and solid dispersions from turbulent gas streams: a stochastic model. *Chem. Engng Sci.* **26**, 419–439.

HUTCHINSON, P., BUTTERWORTH, D. & OWEN, R. G. 1974 Development of a model for horizontal annular flow. UKAEA Report No. AERE-R 7789.

JAMES, P. W., WHALLEY, P. B. & HEWITT, G. F. 1980 Droplet motion in two-phase flow. Presented at *ANS/ASME/NRC Int. topic. Mtg on Nuclear Reactor Thermal Hydraulics*, Saratoga Springs, N.Y. Report NUREG/CP-0014, Vol. 2, pp. 1484–1503.

LAURINAT, J. E., HANRATTY, T. J. & JEPSON, W. P. 1985 Film thickness distribution for gas–liquid annular flow in a horizontal pipe. *Phys. Chem. Hydrodynam.* **6**, 179–195.

LIN, T. F., JONES, O. C. JR, LAHEY, R. T. JR, BLOCK, R. C. & MURASE, M. 1985 Film thickness measurements and modelling in horizontal annular flows. *Phys. Chem. Hydrodynam.* **6**, 197–206.

PEARCE, D. L. 1978 Development of the horizontal annular flow model: axial shear stress at the wall. CEGB Report No. RD/L/N, 78/77.

WHALLEY, P. B., HUTCHINSON, P. & HEWITT, G. F. 1974 The calculation of critical heat flux in forced convection boiling. *5th Int. Heat Transfer Conf.* Tokyo, Paper B6.11.

WHALLEY, P. B., HUTCHINSON, P. & JAMES, P. W. 1978 The calculation of critical heat flux in complex situations using an annular flow model. *6th Int. Heat Transfer Conf.*, Toronto, Paper NR-12.

WHALLEY, P. B., HEWITT, G. F. & TERRY, J. W. 1979 Photographic studies of two-phase flow using a parallel light technique. UKAEA Report No. AERE-R 9389.

APPENDIX A

Derivation of Bounds on (θ, t)

Let $g(s)$ be defined by

$$g(s) = \mu^2 V^4 t^2 s^2 - s(2\mu V^2 R^2 t(\cos\theta + \cos\phi) + \mu^2 V^4 t^3) + 2R^4[1 + \cos(\theta + \phi)] + 2\mu V^2 R^2 t^2 \cos\phi. \quad [A.1]$$

We require that $g(s)$ satisfies the inequality

$$g(s) \geqslant 0, \quad [A.2]$$

for s in the interval $(0, t)$.

$g(s)$ has a minimum at $s = s^*$, the root of $dg/ds = 0$, so that s^* is given by

$$s^* = \frac{t}{2} + \frac{R^2(\cos\theta + \cos\phi)}{\mu V^2 t}. \quad [A.3]$$

We consider first the case $(\cos\theta + \cos\phi) > 0$. If $s^* < t$, then we must have $g(s^*) \geqslant 0$. Alternatively, if $s^* > t$ then we must have $g(t) \geqslant 0$. Now

$$g(s^*) = R^4(\sin\theta - \sin\phi)^2 + \mu V^2 R^2 t^2(\cos\phi - \cos\theta) - \frac{\mu^2 V^4 t^4}{4}, \quad [A.4]$$

and so

$$g(s^*) \geqslant 0 \quad \text{if} \quad t^2 \leqslant \frac{4R^2}{\mu V^2} \sin\frac{\theta - \phi}{2}\left(\sin\frac{\theta + \phi}{2} \pm 1\right), \quad [A.5]$$

(whichever is positive);

$$g(t) = 2R^4[1 + \cos(\theta + \phi)] - 2\mu V^2 R^2 t^2 \cos\theta \quad [A.6]$$

so that

$$g(t) \geqslant 0 \quad \text{if} \quad t^2 \leqslant \frac{R^2[1+\cos(\theta+\phi)]}{\mu V^2 \cos\theta}; \tag{A.7}$$

$$s^* < t \quad \text{if} \quad t^2 > \frac{2R^2(\cos\theta+\cos\phi)}{\mu V^2}. \tag{A.8}$$

We thus have the following:

$$\text{if} \quad t^2 < \frac{2R^2(\cos\theta+\cos\phi)}{\mu V^2}$$

then we need

$$t^2 < \frac{R^2[1+\cos(\theta+\phi)]}{\mu V^2 \cos\theta} \tag{A.9}$$

and if

$$t^2 > \frac{2R^2(\cos\theta+\cos\phi)}{\mu V^2}$$

then we need

$$t^2 < \frac{4R^2}{\mu V^2}\sin\frac{\theta-\phi}{2}\left(\sin\frac{\theta+\phi}{2} \pm 1\right). \tag{A.10}$$

Secondly, we consider the case $(\cos\theta+\cos\phi) < 0$. For this case if $s^* \geqslant 0$ then we must have $g(s^*) \geqslant 0$. Alternatively if $s^* < 0$ then we must have $g(0) \geqslant 0$.

$$g(0) = 2R^4[1+\cos(\theta+\phi)] + 2\mu V^2 R^2 t^2 \cos\phi. \tag{A.11}$$

If $\cos\phi > 0$ then $g(0) > 0 \,\forall\, t$ but if $\cos\phi < 0$ then $g(0) > 0$ only if $t^2 < [\![-\{R^2[1+\cos(\theta+\phi)]\}(\mu V^2 \cos\phi)]\!]$:

$$s^* > 0 \quad \text{if} \quad t^2 > -\frac{2R^2(\cos\theta+\cos\phi)}{\mu V^2}. \tag{A.12}$$

We thus have the following:

$$\text{if} \quad t^2 < -\frac{2R^2(\cos\theta+\cos\phi)}{\mu V^2}$$

then we need

$$t^2 < -\frac{R^2[1+\cos(\theta+\phi)]}{\mu V^2 \cos\phi} \tag{A.13}$$

when $\cos\phi < 0$, and if

$$t^2 > -\frac{2R^2(\cos\theta+\cos\phi)}{\mu V^2}$$

then we need

$$t^2 < \frac{4R^2}{\mu V^2}\sin\frac{\theta-\phi}{2}\left(\sin\frac{\theta+\phi}{2} \pm 1\right). \tag{A.14}$$

APPENDIX B

Existence and Uniqueness of Solutions to [91]

Equation [91] can be integrated to give the linear homogeneous integral equation

$$\eta(\theta) = \int_0^{\pi} K(\theta;\chi)\,\eta(\chi)\,d\chi, \tag{B.1}$$

subject to the boundary condition

$$\eta(0) = 1, \tag{B.2}$$

where the kernel $K(\theta;\chi)$ is given by

$$K(\theta;\chi)=\frac{1}{\sin\theta\tan^{\lambda}\left(\frac{\theta}{2}\right)}\int_0^{\theta}\lambda\tan^{\lambda}\left(\frac{\psi}{2}\right)P(\psi;\chi)\,d\psi, \qquad [B.3]$$

and $P(\psi;\chi)$ is defined by

$$P(\psi;\chi)=p(\psi;\chi)+p(2\pi-\psi;\chi). \qquad [B.4]$$

We note that the kernel satisfies the constraint

$$\int_0^{\pi}K(\theta;\chi)\,d\theta=1, \qquad [B.5]$$

independently of χ, and is positive for all values of θ and χ.

We consider the space of integrable functions on $[0,\pi]$, i.e. $L'([0,\pi])$ subject to the constraint

$$\int_0^{\pi}\eta(\chi)\,d\chi=1. \qquad [B.6]$$

In this space we consider the operator $\mathcal{K}$ defined by

$$(\mathcal{K}\eta)(\theta)=\int_0^{\pi}K(\theta;\chi)\,\eta(\chi)\,d\chi, \qquad [B.7]$$

which maps the space into itself.

We also define the functions $L(\theta)$ and $M(\theta;\chi)$ by

$$L(\theta)=\min_{\chi\in[0,\pi]}K(\theta;\chi) \qquad [B.8]$$

and

$$M(\theta;\chi)=K(\theta;\chi)-L(\theta), \qquad [B.9]$$

so that $L(\theta)$ and $M(\theta;\chi)$ are positive for all values of θ and χ and satisfy the relations

$$\int_0^{\pi}L(\theta)\,d\theta=l>0 \qquad [B.10]$$

and

$$\int_0^{\pi}M(\theta;\chi)\,d\theta=1-l>0. \qquad [B.11]$$

Using these relations it follows that

$$\left\|(\mathcal{K}\eta_1)(\theta)-(\mathcal{K}\eta_2)(\theta)\right\|=\int_0^{\pi}\left|\int_0^{\pi}K(\theta;\chi)\,[\eta_1(\chi)-\eta_2(\chi)]\,d\chi\right|d\theta,$$

$$\leqslant(1-l)\int_0^{\pi}\left|\eta_1(\chi)-\eta_2(\chi)\right|d\chi=(1-l)\left\|\eta_1-\eta_2\right\|. \qquad [B.12]$$

Hence the operator $\mathcal{K}$ is a contraction and using the contraction mapping principle it follows that there exists a unique solution to [B.1] subject to the constraint [B.6]. However, noting that provided there is some deposition at the top of the tube $\eta(0)\neq 0$, it follows by renormalization that there exists a unique solution to [B.1] subject to the boundary condition [B.2].

APPENDIX C

Numerical Solution Scheme for [91]

Remembering that

$$\int_0^{2\pi}p(\theta;\chi)\,\eta(\chi)\,d\chi=\int_0^{\pi}P(\theta;\chi)\,\eta(\chi)\,d\chi, \qquad [C.1]$$

where

$$P(\theta;\chi)=p(\theta;\chi)+p(2\pi-\theta;\chi), \qquad [C.2]$$

we may write [91] as

$$\frac{\mathrm{d}}{\mathrm{d}\theta}[\eta(\theta)\sin\theta]+\lambda\eta(\theta)=\lambda\int_0^{\pi}P(\theta;\chi)\,\eta(\chi)\,\mathrm{d}\chi \qquad [C.3]$$

with

$$\eta(\theta)=1 \quad \text{at} \quad \theta=0 \quad \text{and} \quad 0\leqslant\theta,\chi\leqslant\pi. \qquad [C.4]$$

The range $[0,\pi]$ is subdivided into N intervals of length $\delta=\pi/N$ and the approximate numerical solution to [C.3] will be obtained at the $(N+1)$ grid points

$$\theta_i=(i-1)\,\delta, \quad i=1,2,\ldots,N+1.$$

We approximate the derivative term in [91] by its finite-difference approximation centred on the point $\theta_{i+1/2}=(i-\frac{1}{2})\,\delta$,

$$\frac{\mathrm{d}}{\mathrm{d}\theta}[\eta(\theta)\sin\theta]\approx\frac{\eta_{i+1}\sin\theta_{i+1}-\eta_i\sin\theta_i}{\delta}, \quad i=1,\ldots,N, \qquad [C.5]$$

where $\eta_i=\eta(\theta_i)$, and approximate the integral term by using the trapezium rule, again centred on $\theta_{i+1/2}$:

$$\int_0^{\pi}P(\theta;\chi)\,\eta(\chi)\,\mathrm{d}\chi=\frac{\delta}{4}\sum_{j=1}^{N}\left(P_{i,j}\eta_j+P_{i,j+1}\eta_{j+1}+P_{i+1,j}\eta_j+P_{i+1,j+1}\eta_{j+1}\right),$$

where $P_{i,j}=P(\theta_i,\chi_j)$.

The finite-difference approximation to [C.3] now becomes

$$\eta_{i+1}\left(\sin\theta_{i+1}+\frac{\lambda\delta}{2}\right)-\eta_i\left(\sin\theta_i-\frac{\lambda\delta}{2}\right)=\frac{\lambda\delta^2}{4}\sum_{j=1}^{N}\left[\eta_{j+1}\left(P_{i+1,j+1}+P_{i,j+1}\right)+\eta_j\left(P_{i+1,j}+P_{i,j}\right)\right], \quad i=1,\ldots N. \qquad [C.6]$$

There are N equations in the N unknowns $\eta_2\ldots\eta_{N+1}$ but the equations are not linearly independent, because

$$\frac{\delta}{2}\sum_{i=1}^{N}\left(P_{i,j}+P_{i+1,j}\right)=1, \quad \forall j. \qquad [C.7]$$

One further equation is required and we obtain it by assuming that $\mathrm{d}/\mathrm{d}\theta\,(\eta(\theta)\sin\theta)\to 0$ as $\theta\to 0$. This assumption enables us to derive the further equation

$$\eta_1(1+\lambda)=\frac{\lambda\delta}{2}\sum_{j=1}^{N}\left(P_{1,j}\eta_j+P_{1,j+1}\eta_{j+1}\right), \qquad [C.8]$$

from the limiting form of [C.1] as $\theta\to 0$.

The above finite-difference equations are now cast in the form

$$A_{ij}X_j=B_j, \quad i,j=1,\ldots,N, \qquad [C.9]$$

with

$$X_j=\eta_{j+1}, \qquad [C.10]$$

$$B_i=\frac{\lambda\delta^2}{4}\cdot\eta_1\left(P_{i+1,1}+P_{i,1}\right), \quad i=2,\ldots,N, \qquad [C.11]$$

$$B_1=\frac{2\eta_1}{\lambda\delta}(1+\lambda)-P_{i,1}, \qquad [C.12]$$

$$A_{ij} = -\frac{\lambda\delta^2}{2}\left(P_{i,j+1} + P_{i+1,j+1}\right) + \left(\sin\theta_i + \frac{\lambda\delta}{2}\right)\delta_{i,j} + \left(\frac{\lambda\delta}{2} - \sin\theta_i\right)\delta_{i,j+1} + \frac{\lambda\delta^2}{4}\left(P_{i,j+1} + P_{i+1,j+1}\right)\delta_{j,N}, \quad i = 2, \ldots, N, \quad \text{[C.13]}$$

and

$$A_{1j} = 2\,P_{1,j+1} - P_{1,j+1}\,\delta_{j,N}, \quad \text{[C.14]}$$

where

$$\delta_{M,L} = 0 \quad \text{if} \quad M \neq L \quad \text{[C.15]}$$
$$= 1 \quad \text{if} \quad M = L.$$

These equations are then solved using the Harwell Subroutine Library Program MA21. A similar scheme using simple backward differences has also been used but the above scheme is more accurate.